PARIS
19TH TEXAS SYMPOSIUM

Recent results from the AGASA experiment

M. Takeda[1], N. Hayashida[1], K. Honda[2], N. Inoue[3], K. Kadota[4], F. Kakimoto[4], K. Kamata[5], S. Kawaguchi[6], Y. Kawasaki[7], N. Kawasumi[8], E. Kusano[3], Y. Matsubara[9], K. Murakami[10], M. Nagano[11], D. Nishikawa[1], H. Ohoka[1], S. Osone[1], N. Sakaki[1], M. Sasaki[1], K. Shinozaki[3], N. Souma[3], M. Teshima[1], R. Torii[1], I. Tsushima[8], Y. Uchihori[12], T. Yamamoto[1], S. Yoshida[1], and H. Yoshii[13]

(1) Institute for Cosmic Ray Research, University of Tokyo, Tokyo 188-8502, Japan
(2) Faculty of Engineering, Yamanashi University, Kofu 400-8511, Japan
(3) Department of Physics, Saitama University, Urawa 338-8570, Japan
(4) Department of Physics, Tokyo Institute of Technology, Tokyo 152-8551, Japan
(5) Nishina Memorial Foundation, Komagome, Tokyo 113-0021, Japan
(6) Faculty of General Education, Hirosaki University, Hirosaki 036-8560, Japan
(7) Department of Physics, Osaka City University, Osaka 558-8585, Japan
(8) Faculty of Education, Yamanashi University, Kofu 400-8510, Japan
(9) Solar-Terrestrial Environment Laboratory, Nagoya University, Nagoya 464-8601, Japan
(10) Nagoya University of Foreign Studies, Nissin, Aichi 470-0131, Japan
(11) Department of Applied Physics and Chemistry, Fukui Institute of Technology, Fukui 910-8505, Japan
(12) National Institute of Radiological Sciences, Chiba 263-8555, Japan
(13) Department of Physics, Ehime University, Matsuyama 790-8577, Japan

Abstract. The cosmic-ray energy spectrum above 3×10^{18}eV is reported using the updated data set of the Akeno Giant Air Shower Array (AGASA) from February 1990 to August 1998. The energy spectrum extends beyond the expected GZK cutoff and 7 cosmic rays are observed above 10^{20}eV. Arrival direction distribution of extremely high energy cosmic rays has also studied using not only the AGASA data set but also the Akeno 20 km^2 array data set. While no significant large-scale anisotropy is found on the celestial sphere, some interesting clusters of cosmic rays are observed. Above 4×10^{19}eV, there are one triplet and three doublets within separation angle of 2.5° and the probability of observing these clusters by a chance coincidence under an isotropic distribution is smaller than 1 %. Especially the triplet is observed against expected 0.05 events. The $\cos(\theta_{GC})$ distribution expected from the Dark Matter Halo model fits the data as well as an isotropic distribution above 2×10^{19}eV and 4×10^{19}eV, but is a poorer fit than isotropy above 10^{19}eV. Arrival direction distribution of seven 10^{20}eV cosmic rays is consistent with that of lower energy cosmic rays and is uniform. Three of seven are members of doublets above about 4×10^{19}eV.

1. Introduction

Investigation on energy spectrum and anisotropy of extremely high energy cosmic rays are the most important aspects to reveal their origin. The energy spectrum has two informative energies: $E \simeq 10^{19}$eV and 4×10^{19}eV. The former is the energy where the spectral slope changes [1, 2, 3, 4, 5]. This is interpreted as transition from galactic to extragalactic origin. The latter is the energy where the GZK effect [6, 7], which

is a series of energy loss through interaction with the cosmic microwave background photons, becomes important on their propagation from sources. The spectral features around these energies reflect origin, acceleration mechanism and propagation process of extremely high energy cosmic rays [8, 9, 10].

It is also important to study whether their arrival direction distribution changes at these energies. If cosmic rays with energies $\gtrsim 10^{19}$eV are protons of galactic origin they slightly deflect in the galactic magnetic field, so that one could observe the correlation of their arrival directions with the galactic structure. Especially in the highest observed energy range, correlation of cosmic rays with the local structure of galaxies may be expected if their origins are nearby astrophysical objects and the intergalactic magnetic field is less than 10^{-9} gauss. Since the distance to sources of cosmic rays above the expected GZK cutoff is limited to 50 Mpc [8, 9, 10], their arrival directions may be correlated with luminous matter distribution if they are astrophysical source origin such as hot spots of radio galaxies [11, 12, 13, 14], active galactic nuclei [15, 16, 17], accretion flow to a cluster of galaxies [18], relativistic shocks in gamma-ray bursts [19, 20], and so on. There is another possibility that most energetic cosmic rays are generated through decay of supermassive "X" particles related to topological defects ([21], reference therein). In this case, arrival directions of most energetic cosmic rays are not necessarily associated with luminous matters. If such particles are the part of Dark Matter and are concentrated in the galactic halo, anisotropy associated with our galactic halo is expected [22, 23].

In this paper, we first show the updated energy spectrum above 3×10^{18}eV using the data set of the Akeno Giant Air Shower Array (AGASA) until August 1998. Then we search for cosmic-ray anisotropy with the additional data set of the Akeno 20 km^2 array (A20) before 1990.

2. Experiment

The Akeno Observatory is situated at 138° 30′ E and 35° 47′ N. AGASA consists of 111 surface detectors deployed over an area of about 100 km^2, and has been in operation since 1990 [24, 25]. A20 is a prototype detector system of AGASA, operated from 1984 to 1990 [26], and is a part of AGASA after 1990.

Each surface detector consists of plastic scintillators of 2.2 m^2 area. The detectors are placed with a separation of about 1 km. They are controlled and operated from a central computer through optical fiber network. Relative time difference among the detectors are measured with 40 nsec accuracy; all clocks at detector sites are synchronized to the central clock and signal-propagation time in cables and electronic devices are regularly measured at start of each run (twice a day). The details of the AGASA instruments have been described in Chiba et al. (1992) [24] and Ohoka et al. (1997) [25].

It is well established that local density of charged air shower particles at a specific distance is a good energy estimator [27], since this depends weakly on variation in the interaction model, fluctuation in shower development and primary mass. In the AGASA experiment, we adopt local density $S(600)$ at 600 m which is determined from fitting the lateral distribution of observed particle densities to an empirical formula [28]. This empirical formula is found to be valid for EAS with energies up to 10^{20} eV [29, 30]. The conversion relation from $S(600)$ to the primary energy is evaluated

through the Monte Carlo simulation [31] up to 10^{19} eV by

$$E = 2.03 \times 10^{17}\, S_0(600) \quad eV,$$

where $S_0(600)$ is the $S(600)$ value in units of m^{-2} for a vertically incident shower. Since inclined air showers traverse more atmospheric depth than vertical showers, $S_\theta(600)$ observed with zenith angle θ must be transformed into $S_0(600)$ at the vertical. This attenuation curve of $S(600)$ has been formulated by Yoshida et al. (1994) [28].

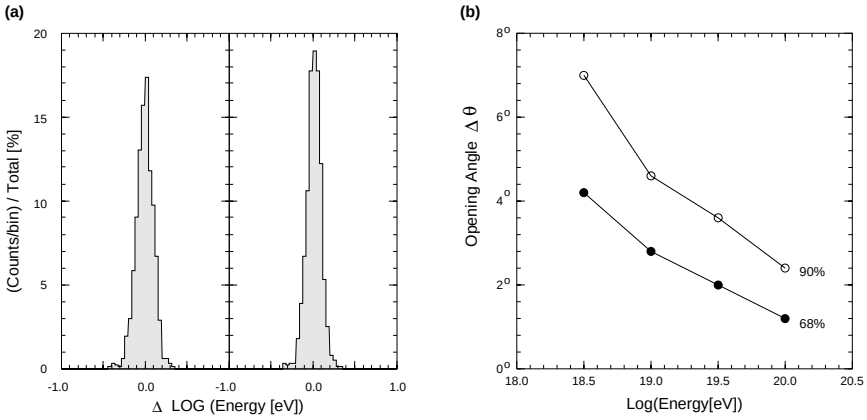

Figure 1. Accuracy of event reconstruction. (a) Fluctuation of energy determination for $10^{19.5}$ eV (left) and 10^{20} eV (right) showers with zenith angles less than 45°. (b) Accuracy on arrival direction determination. Closed and open circles are the opening angles encompassed 68 % and 90 % data.

The accuracy on determination of shower parameters are evaluated through the analysis of a large number of artificial events. These artificial events are generated with taking account of air shower features and fluctuation determined experimentally. Figure 1(a) shows the accuracy on arrival direction determination for cosmic-ray induced air showers as a function of energies. The vertical axis denotes the opening angle $\Delta\theta$ between input (simulated) and output (analyzed) arrival directions. The opening angles including 68 % and 90 % of data are plotted. By analyzing artificial events with the same algorithm used above, the accuracy on energy determination is estimated to be ± 30 % above 10^{19}eV as shown in Figure 1(b).

Table 1. Number of events in the A20 and AGASA data sets

Array	$\geq 1 \times 10^{19}$eV	$\geq 4 \times 10^{19}$eV	$\geq 1 \times 10^{20}$eV
A20	59	7	0
AGASA	522	40	7
Total	581	47	7

Table 1 lists the number of selected events, N(E), with zenith angles smaller than 45° and with core locations inside the array area. Events below 10^{19}eV are used only

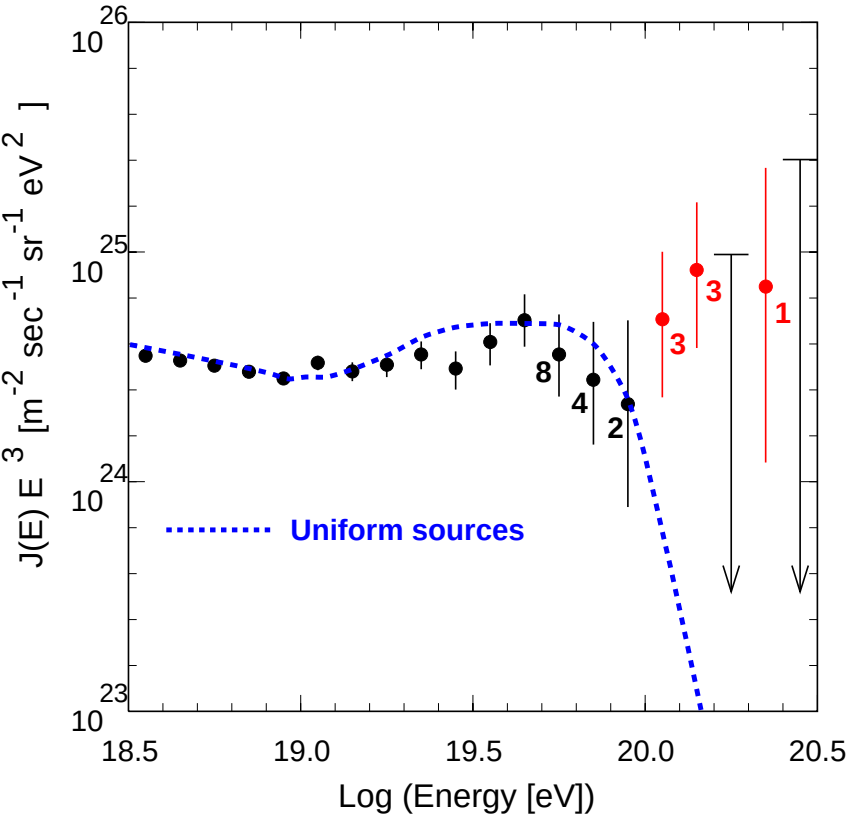

Figure 2. Energy spectrum observed with AGASA. The vertical axis is multiplied by E^3. Error bars represent the Poisson upper and lower limits at 68 % and arrows are 90 % C.L. upper limits. Numbers attached to points show the number of events in each energy bin. The dashed curve represents the spectrum expected for extragalactic sources distributed uniformly in the Universe, taking account of the energy determination error [11].

for a reference analysis in anisotropy study. The difference of N(E $\geq$ 4 $\times$ 10^{19}eV) / N(E $\geq$ 10^{19}eV) between A20 and AGASA arises from the difference of detection efficiency of each system. Seven events are observed above 10^{20}eV, including one event after Takeda et al. (1998) [5].

3. Results

3.1. Energy Spectrum

The updated energy spectrum observed with AGASA, without A20, is shown in Figure 2, multiplied by E^3 in order to emphasize details of the steeply falling spectrum. Error bars represent the Poisson upper and lower limits at 68% and arrows are 90% C.L. upper limits. Numbers attached to points show the number of events in each energy bin. Here, the total exposure above 10^{19}eV is 3.1 $\times$ 10^{16} m^2 sr sec. The dashed curve

represents the spectrum expected for extragalactic sources distributed uniformly in the Universe, taking account of the energy determination error [10].

First, we examine whether the observed energy spectrum could be represented by a single power law spectrum ($\propto E^{-\gamma_1}$). The optimum spectral index γ_1 is derived from the maximum likelihood procedure comparing the observed and expected number of events in each energy bin. This procedure is same as described in Yoshida et al. [4]. The maximum likelihood procedure for a single power law spectrum results in $\gamma_1 = 3.06^{+0.09}_{-0.13}$; the likelihood significance of γ_1 is only 0.09. If only events with energies below $10^{19}eV$ are considered, $\gamma_1(E \leq 10^{19}eV) = 3.24^{\pm 0.11}$ is obtained which is consistent with the spectral index, 3.16 ± 0.08, determined from the Akeno experiment [32].

Next, a broken energy spectrum is examined with the same procedure. The broken energy spectrum is assumed to be

$$\frac{dJ}{dE} = \begin{cases} \kappa\,(E/E_a)^{-\gamma_0} & 3 \times 10^{18}eV \leq E < E_a \\ \kappa\,(E/E_a)^{-\gamma_2} & E_a \leq E \end{cases} ,$$

where γ_0 and γ_2 are indexes below and above a bending (ankle) energy E_a, and γ_0 is fixed to be $\gamma_1(E \leq 10^{19}eV) = 3.16$ determined from the Akeno experiment [32]. The most probable parameters are obtained at $E_a = 10^{19.01}$ eV and $\gamma_2 = 2.73^{+0.32}_{-0.24}$, where the likelihood significance is found to be 0.95. This is also consistent with the results of 2.8 ± 0.3 at energies above $10^{18.8}$ eV determined from the Akeno experiment [32] and of $2.3^{+0.5}_{-0.3}$ above $10^{19.0}$ eV in the previous paper [4].

Furthermore, the energy spectrum presented here extends up to higher energies than the previous results [4, 32]; seven events were observed above 10^{20} eV. If the real energy spectrum is that shown in Figure 2 as the dashed curve, the expected number of events above 10^{20} eV is less than one, taking account of the energy resolution. The energy spectrum is therefore more likely to extend beyond 10^{20} eV without the GZK cutoff.

3.2. Analysis in the Equatorial Coordinates

3.2.1. Harmonic Analysis In order to search for cosmic ray anisotropy, it is required to compare observed and expected event frequencies at each region. An expected frequency is easily estimated as far as the exposure in each direction can be obtained; the uniformity of observation time on solar time for several years, which results in the uniform observation in right ascension, is expected for a surface array detection system operating in stable like AGASA. The fluctuation of the observation time on the local sidereal time is (0.2 ± 0.1) % which is small enough compared with anisotropy in this energy range, so that the exposure (observation time $\times$ collection area) in right ascension is quite uniform.

Figure 3 shows results of the first (left) and second (right) harmonics in right ascension. The amplitude (top), the phase (middle), and the chance probability (bottom) are shown in each energy bin. In the top panels of the harmonic amplitude, the shaded region is expected from statistical fluctuation of an isotropic distribution with the chance probability larger than 10 %. No significant anisotropy above this level is found above 3.2×10^{18}eV. This is consistent with our previous paper [33], in which zenith angles up to 60° were used.

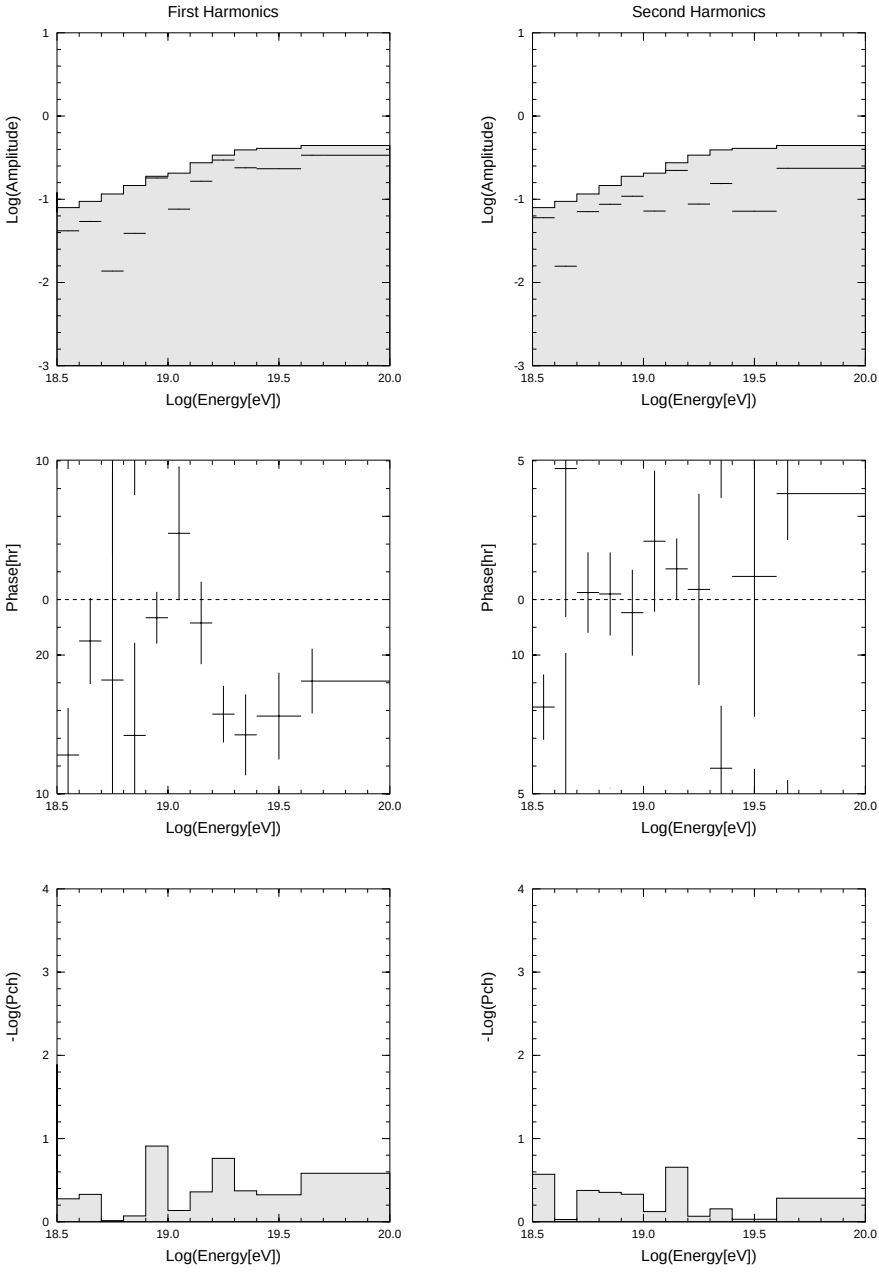

Figure 3. Results of the harmonic analysis. Top to bottom, the amplitude, the phases and the chance probabilities of the first (left) and second (right) harmonics are shown. In the top panels of the harmonic amplitude, the shaded region is expected from statistical fluctuation of an isotropic distribution with the chance probability larger than 10 %.

3.2.2. Declination Distribution Figure 4 shows the declination distribution of events above 10^{19}eV (light shaded histogram) and 10^{20}eV (dark shaded histogram). A solid curve is a third order polynomial function fitted to the light shaded histogram. This curve is consistent with the zenith angle dependence of the AGASA exposure and considered to be the expected distribution if cosmic rays distribute isotropically on the celestial sphere. Since the trigger efficiency is independent of energy above 10^{19}eV and zenith angle less than 45°, this distribution is applied to in higher energies. Excess with 2.5 σ deviation is found in $\delta = [30°, 40°]$ and this will be discussed later.

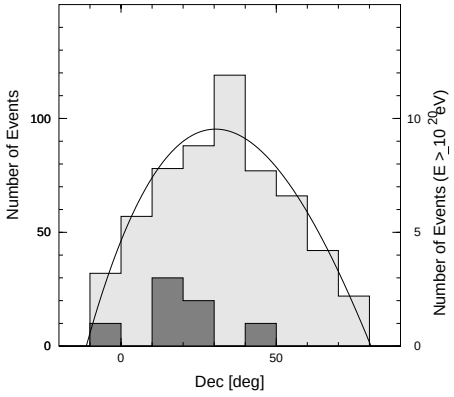

Figure 4. Declination distribution of the observed cosmic rays. (Light shaded histogram: $\geq 10^{19}$eV. Dark shaded histogram: $\geq 10^{20}$eV, the right-had vertical axis should be referred.)

3.3. Analysis in the Galactic and Supergalactic Coordinates

3.3.1. Galactic and Supergalactic Plane Enhancement If cosmic rays have origin associating with nearby astrophysical objects, we may expect cosmic-ray anisotropy correlated with the galactic or supergalactic plane. Figure 5 shows the latitude distribution on the galactic (left) and supergalactic (right) coordinates in three energy ranges of $(1 - 2) \times 10^{19}$eV (top), $(2 - 4) \times 10^{19}$eV (middle), and $\geq 4 \times 10^{19}$eV (bottom). A solid line in each panel indicates the cosmic-ray intensity expected from an isotropic distribution. In order to examine any preference for arrival directions along the galactic and supergalactic planes, the plane enhancement parameter f_E introduced by Wdowczyk and Wolfendale (1984) [34] was used. The f_E value characterizes the anisotropy expressed by:

$$I_{obs}(b)/I_{exp}(b) = (1 - f_E) + 1.402\, f_E\, \exp(-b^2), \quad (1)$$

where b is galactic or supergalactic latitude in radians, $I_{obs}(b)$ and $I_{exp}(b)$ are observed and expected intensities at latitude b. A positive f_E value suggests a galactic or supergalactic plane enhancement, $f_E = 0$ indicates that arrival direction distribution is isotropic, and a negative f_E shows depression around the plane. Figure 6 shows the dependence of f_E on the primary energy for the galactic (left) and supergalactic (right) coordinates. Some excess can be seen around the supergalactic plane in the seventh energy bin (log(E[eV]) = [19.1, 19.2]), where $f_E^{SG} = 0.36 \pm 0.15$. In other energies, the arrival direction distribution is consistent with an isotropic distribution.

3.3.2. θ_{GC} Distribution Figure 7 shows the $\cos(\theta_{GC})$ distribution, where θ_{GC} is the opening angle between the cosmic-ray arrival direction and the galactic center direction, with energies above 10^{19}eV (top), 2×10^{19}eV (middle), and 4×10^{19}eV (bottom). Histograms are the observed distribution and the solid curves are expected from an isotropic distribution. The observed distribution is consistent with the solid

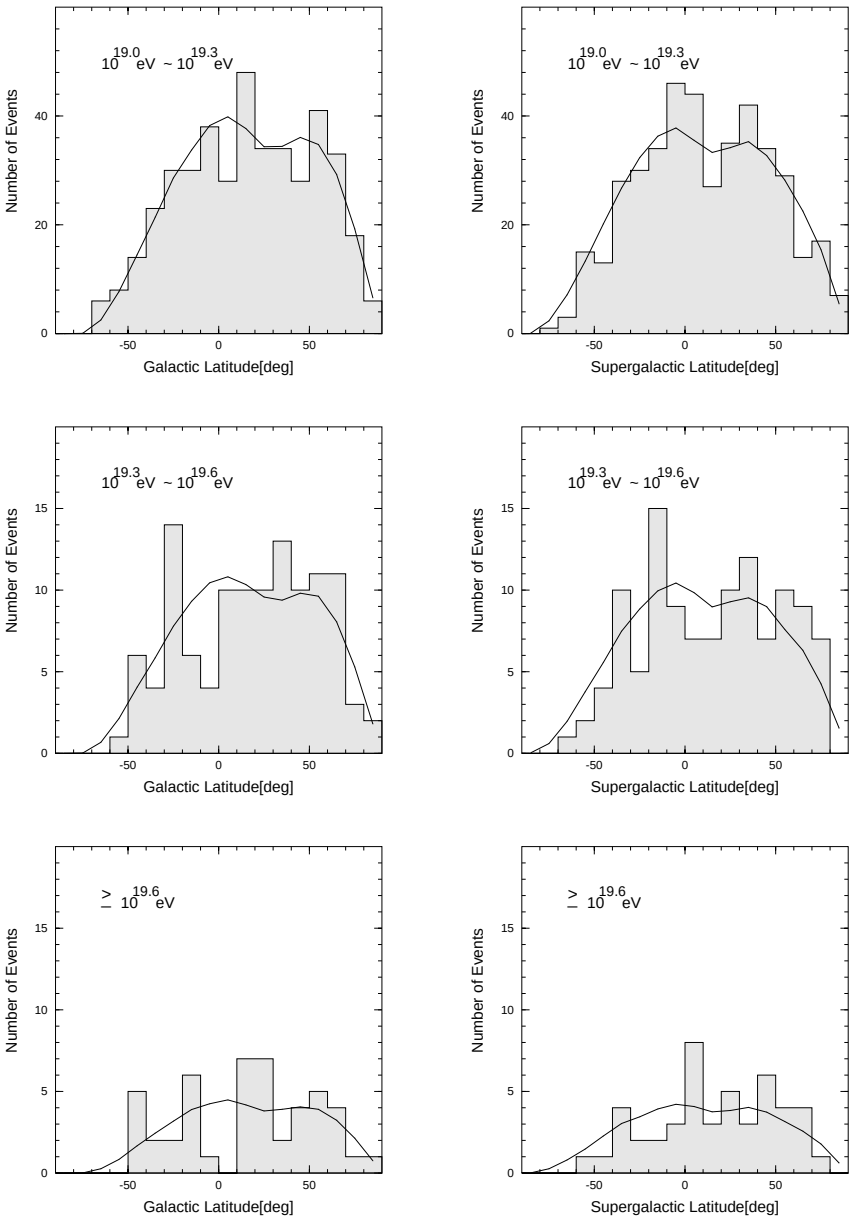

Figure 5. Galactic (left) and supergalactic (right) latitude distribution. (Top: (1 – 2) $\times 10^{19}$eV. Middle: (2 – 4) $\times 10^{19}$eV. Bottom: $\geq 4 \times 10^{19}$eV.)

curve in all energy ranges. The dashed and dotted curves are expected from the Dark Matter Halo model [35] and will be discussed in Section 4.1.

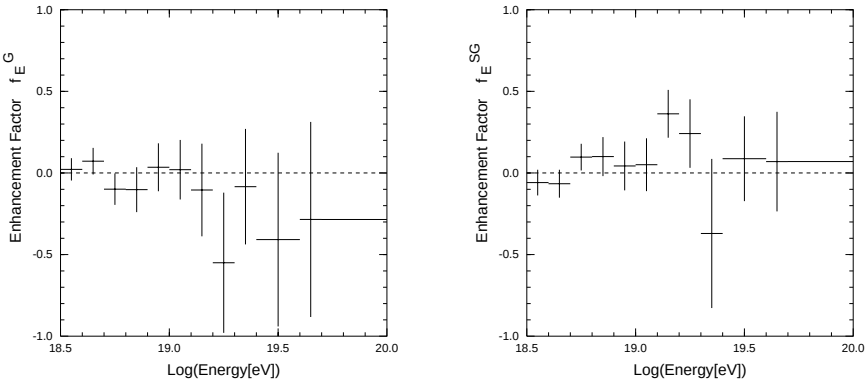

Figure 6. Dependence of the plane enhancement factor on the energy. (Left: for the galactic coordinates. Right: for the supergalactic coordinates)

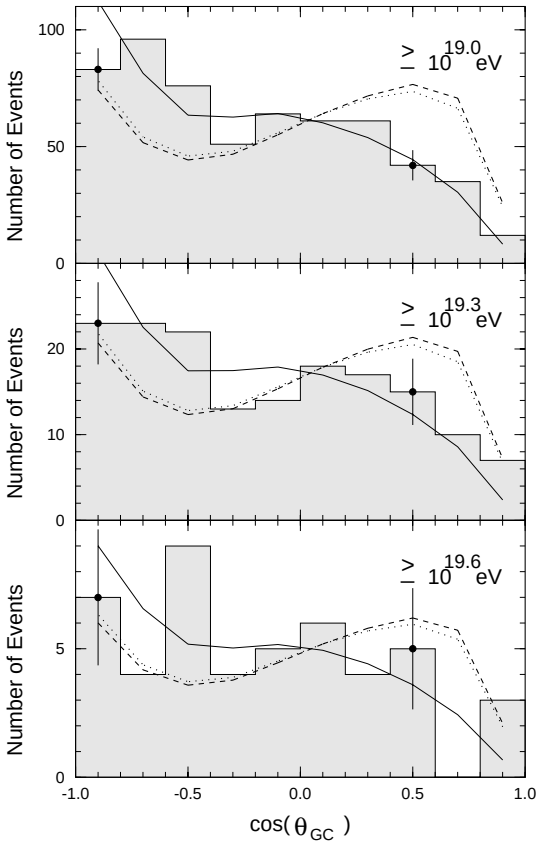

Figure 7. $\cos(\theta_{GC})$ distribution. (Top: $\geq 10^{19}$eV. Middle: $\geq 2 \times 10^{19}$eV. Bottom: $\geq 4 \times 10^{19}$eV.) Here, θ_{GC} is the opening angle between the cosmic-ray direction and the galactic center direction, with energies $\geq 10^{19}$eV (top), 2×10^{19}eV (middle), and 4×10^{19}eV (bottom). The solid, dashed and dotted curves indicate the distribution expected for the isotropic, ISO and NFW models, respectively.

3.4. Significance Map of Cosmic-Ray Excess/Deficit

There is no statistically significant large-scale anisotropy in the above one-dimensional analyses. Here, we search for two-dimensional anisotropy with taking account of the angular resolution event by event.

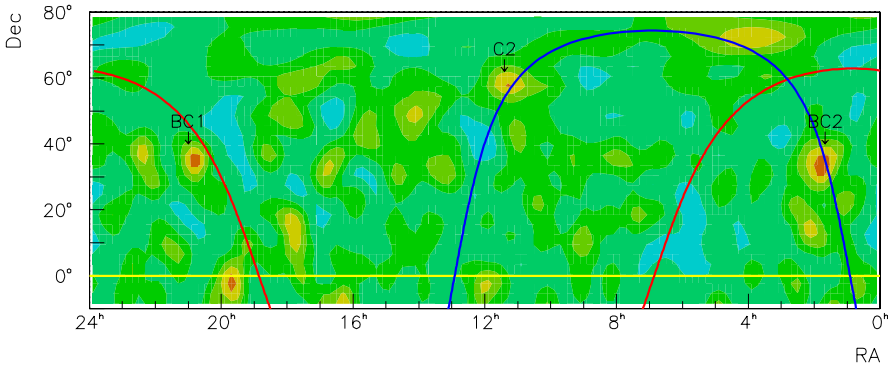

Figure 8. Significance map of cosmic-ray excess/deficit above 10^{19}eV. The dashed and dash-dotted curve indicate the galactic and supergalactic plane, respectively.

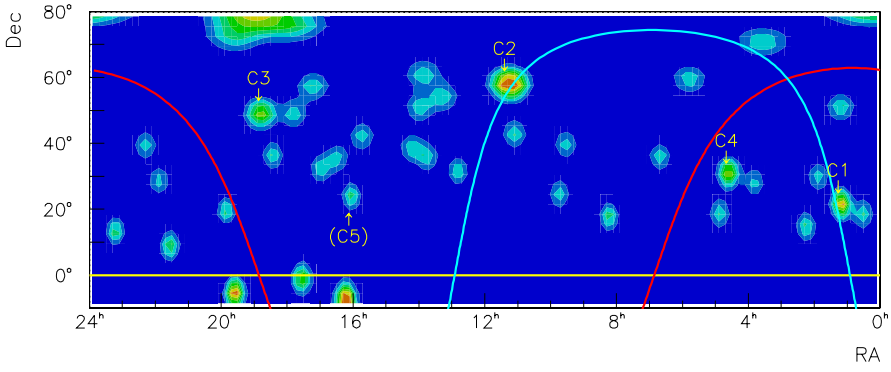

Figure 9. Significance map of cosmic-ray excess/deficit above 4×10^{19}eV. The dashed and dash-dotted curve indicate the galactic and supergalactic plane, respectively.

Figures 8 and 9 show the contour maps of the cosmic-ray excess or deficit with respect to an isotropic distribution above 10^{19}eV and 4×10^{19}eV, respectively. A bright (red) region indicates that the observed cosmic-ray intensity is larger than the expected intensity and a dark (blue) region shows a deficit region. For each observed event, we calculate a point spread function which is assumed to be a normalized Gaussian probability distribution with a standard deviation of the angular resolution

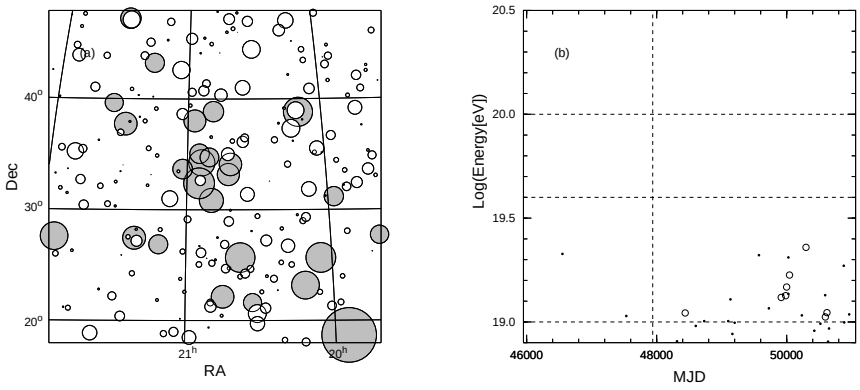

Figure 10. BC1 cluster. (a) Arrival directions of cosmic rays around the BC1 cluster. Radius of each circle corresponds to log(E[eV]), and shaded and open circles have energies above 10^{19}eV and between 3×10^{18}eV and 10^{19}eV, respectively. (b) Arrival time – energy relation. Open circles denote members of the BC1 cluster and dots are cosmic rays near the BC1 cluster. After the vertical dotted line, A20 is combined into AGASA.

$\Delta\theta$ obtained from Figure 1. The probability densities of all events are folded into cells of $1^\circ \times 1^\circ$ in the equatorial coordinates. At each cell, we sum up densities within 4.0° radius for Figure 8 and 2.5° for Figure 9. These radii are obtained from $\sqrt{2} \times \Delta\theta$, and they would make excess regions clearer. The reference distribution is obtained from an isotropic distribution. In these figures, small statistics of observed and expected events result in bright regions at the lower and higher declination and hence bright spots below $\delta = 0^\circ$ are not significant. Two distinctive bright regions are found in Figure 8, which are broader than the angular resolution. They are referred to as broad clusters, such as the BC1 (20^h50^m, 32°) and BC2 (1^h40^m, 35°). The member events within 4° radius of BC1 are listed in Table 2. Four brighter regions in the middle declination are found in Figure 9: the C1 – C4 clusters which are listed in Table 3.

Table 2. Members of the clustering events above 10^{19}eV.

Name	Date	Energy	Coordinates			
			α	δ	l^G	b^G
BC1	95/10/09	1.47×10^{19}eV	$20^h\ 50^m$	30.8°	73.9°	$-\ 8.2^\circ$
	95/11/23	1.68	$20^h\ 54^m$	34.2°	77.1°	$-\ 6.8^\circ$
	95/07/18	1.31	$20^h\ 42^m$	33.2°	74.8°	$-\ 5.5^\circ$
	95/09/24	1.33	$20^h\ 41^m$	34.1°	75.4°	$-\ 4.8^\circ$
	91/07/02	1.10	$20^h\ 55^m$	35.1°	77.9°	$-\ 6.4^\circ$
	96/08/02	2.29	$20^h\ 55^m$	32.4°	75.9°	$-\ 8.1^\circ$
	97/05/28	1.06	$20^h\ 50^m$	34.7°	77.1°	$-\ 5.9^\circ$
	97/06/20	1.11	$21^h\ 02^m$	33.7°	77.8°	$-\ 8.4^\circ$
BC2			$1^h\ 40^m$	35°	134°	-27°

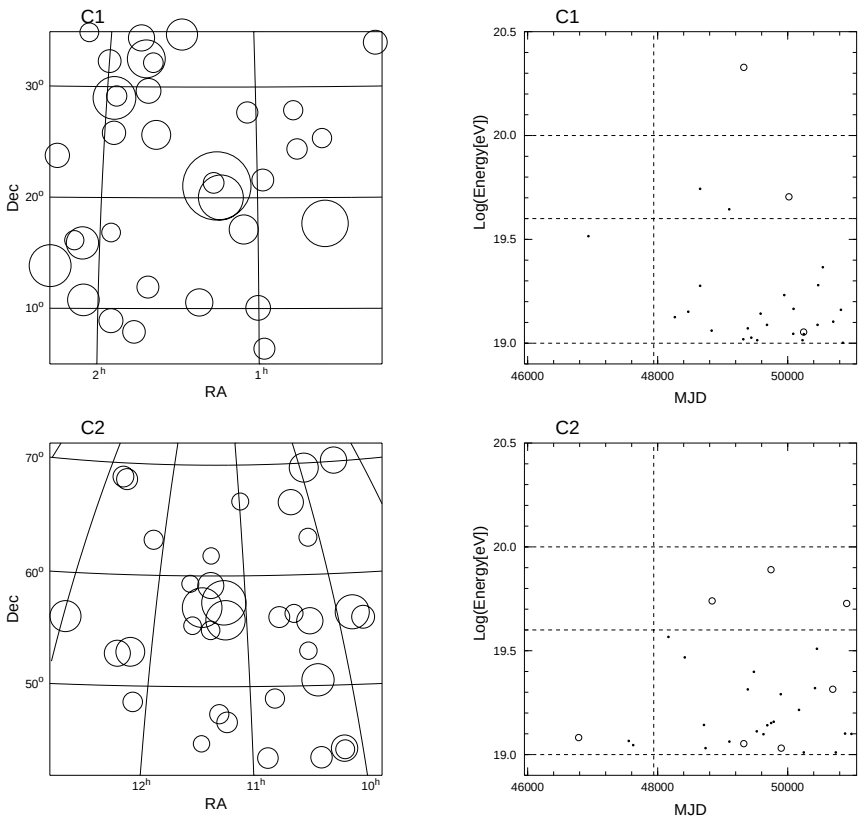

Figure 11. Arrival directions and arrival time – energy relation for the C1 and C2 clusters. Here, cosmic rays above 10^{19}eV are plotted. (See also Figure 10)

The C1 – C3 clusters follow the notation used in our previous analysis [36]. The C2 cluster is observed in both energy ranges.

In Figure 8, the contour map has eight steps in $[-3\sigma, +3\sigma]$; lower two steps below -1.5σ are absent. The significance of deviation from an isotropic distribution are estimated to be 2.4 σ at the C2 cluster, 2.7 σ at the BC1 cluster, and 2.8 σ at the BC2 cluster. The arrival directions of cosmic rays around the BC1 cluster are shown in Figure 10(a), and a radius of each circle corresponds to the logarithm of its energy. Shaded circles have energies above 10^{19}eV and open circles below 10^{19}eV. Figure 10(b) shows the arrival time – energy relation, and open circles denote members of the BC1 cluster. The members of the BC1 cluster have energies between 10^{19}eV and 2.5 $\times$ 10^{19}eV and no excess of cosmic rays are observed below 10^{19}eV around this direction. Five members of the BC1 cluster are observed around MJD 50,000. This cluster is in the direction of a famous supernova remnant — the Cygnus Loop which extends about 3° around (20^h50^m, 30° 34′). The BC2 cluster is the broader cluster without a clear boundary. The BC1 and BC2 clusters contribute the excess around $\delta = 35°$ shown in Figure 4. The C2 and BC2 clusters are located near the supergalactic plane and lead the largest f_E^{SG} value in Section 3.3.1.

For small statistics of observed events, Figure 9 reflects the arrival directions of individual events. The brightest peak is at the C2 cluster where three cosmic rays

Table 3. Members of the clustering events above 4×10^{19}eV.

Name	Date	Energy	Coordinates			
			α	δ	l^G	b^G
C1	93/12/03	$\underline{21.3} \times 10^{19}$eV	$1^h\ 15^m$	21.1°	130.5°	−41.4°
	95/10/29	5.07	$1^h\ 14^m$	20.0°	130.2°	−42.5°
C2	92/08/01	5.50	$11^h\ 29^m$	57.1°	143.2°	56.6°
	95/01/26	7.76	$11^h\ 14^m$	57.6°	145.5°	55.1°
	98/04/04	5.35	$11^h\ 13^m$	56.0°	147.5°	56.2°
C3	91/04/20	4.35	$18^h\ 59^m$	47.8°	77.9°	18.4°
	94/07/06	$\underline{10.6}$	$18^h\ 45^m$	48.3°	77.6°	20.9°
C4	86/01/05	5.47	$4^h\ 38^m$	30.1°	170.4°	−11.2°
	95/11/15	4.89	$4^h\ 41^m$	29.9°	171.1°	−10.8°
C5	96/01/11	$\underline{14.4}$	$16^h\ 06^m$	23.0°	38.9°	45.8°
	97/04/10	(3.89)	$15^h\ 58^m$	23.7°	39.1°	47.8°

are observed against expected 0.05 events. It is possible that some of these clusters are observed by a chance coincidence. It should be noted, however, that two of these clusters — the doublet (C1) including the AGASA highest energy event and the triplet (C2) — lie near the supergalactic plane, as pointed in our previous analysis [36]. The arrival directions (left) and arrival time – energy relation (right) for the C1 (top) and C2 (bottom) clusters are shown in Figure 11. A radius of each circle in the left panels corresponds to the logarithm of its energy, and open circles in the right panels denote members of the C1 and C2 clusters. Around the C2 cluster, several lower energy cosmic rays are observed very close to the C2 cluster.

3.5. Cluster Analysis

The threshold energy of 4×10^{19}eV is one distinctive energy where the GZK effect becomes large as mentioned in Section 1. It is, however, quite important to examine what kind of dependence on threshold energy is operating.

To begin with, we estimate the chance probability of observing one triplet and three doublets from 47 cosmic rays above 4×10^{19}eV. A cluster of cosmic rays is defined as follows:

(i) Define the i-th event;

(ii) Count the number of events within a circle of radius 2.5° centered on the arrival direction of the i-th event;

(iii) If this number of events exceeds a certain threshold value N_{th}, the i-th event is counted as a cluster.

This procedure was repeated for total 47 events and then the total number of clusters with N_{th} was determined. The chance probability P_{ch} of observing this number of clusters under an isotropic distribution is obtained from the distribution of the number of clusters using 10,000 simulated data sets. These simulated data sets

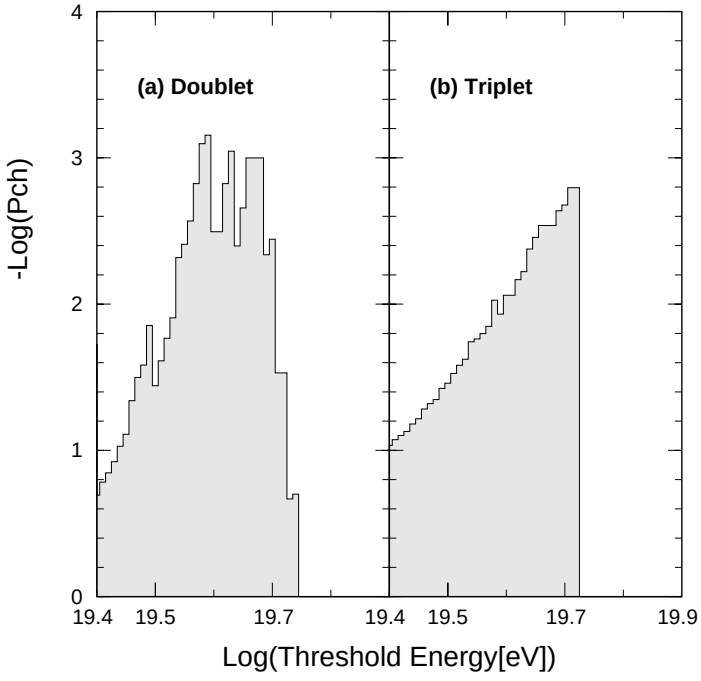

Figure 12. Energy dependence of the chance probability of observing (a) doublets and (b) triplets.

were also analyzed by the same procedure described above. Out of 10,000 simulations, 32 trials had equal or more doublets ($N_{th} = 2$) than the observed data set, so that $P_{ch} = 0.32\%$. And $P_{ch} = 0.87\%$ for triplets ($N_{th} = 3$).

Then, the energy dependence for observing (a) doublets and (b) triplets are estimated and the results are shown in Figure 12. When a new cluster is added above a threshold energy, a histogram changes discontinuously at that energy. At the maximum threshold energy where the triplet is detected, we find $P_{ch} = 0.16$ % in Figure 12(b). The narrow peaks of $P_{ch} \simeq 0.1$ % above 4×10^{19}eV in Figures 12(a) result from the C1, C3 and C4 doublets, and another doublet C5 is found just below 4×10^{19}eV. Here, these chance probabilities are estimated without taking the degree of freedom on the threshold energy into account. However, the chance probabilities are smaller than 1 % and don't vary abruptly with energies above 4×10^{19}eV. This means that the threshold energy of 4×10^{19}eV for doublet and triplet in Figure 9 may indicate any critical energy, and suggests that their sources are not very far being different from those below this energy.

3.6. 10^{20} eV Events

Seven events have been observed with energies above 10^{20}eV, and their energies and coordinates are listed in Table 4. Their declination are near $\delta \simeq 20^\circ$ while an isotropic distribution is shown by the solid curve in Figure 4. To check whether these seven events distribute isotropically or not, we compare celestial distribution of seven 10^{20}eV events with that for events between 10^{19}eV and 10^{20}eV in ten different coordinates.

Table 4. AGASA 10^{20}eV events.

Date	Energy	Coordinates			
		α	δ	l^G	b^G
93/01/12	1.01×10^{20}eV	$8^h\ 17^m$	16.8°	206.7°	26.4°
93/12/03	2.13	$1^h\ 15^m$	21.1°	130.5°	−41.4°
94/07/06	1.06	$18^h\ 45^m$	48.3°	77.6°	20.9°
96/01/11	1.44	$16^h\ 06^m$	23.0°	38.9°	45.8°
96/10/22	1.05	$19^h\ 54^m$	18.7°	56.8°	−4.8°
97/03/30	1.50	$19^h\ 38^m$	−5.8°	33.1°	−13.1°
98/06/12	1.20	$23^h\ 16^m$	12.3°	89.5°	−44.3°

The Kolmogorov-Smirnov (KS) test [37] was used for avoiding any binning effect. The results are summarized in Table 5. The smallest KS probability in Table 5 is 2.5 % for the declination distribution; but this probability becomes larger using data set above 6.3×10^{19}eV. One interesting feature is that five 10^{20}eV cosmic rays come from south-west of the AGASA array, where the strength of the geomagnetic field component which is perpendicular to an air shower axis is larger than the other directions [38].

Table 5. Kolmogorov-Smirnov test for celestial coordinates.

	KS-Probability
Azimuth Angle (ϕ)	0.268
Zenith Angle (θ)	0.867
Right Ascension (α)	0.202
Declination (δ)	0.025
Ecliptic Longitude	0.085
Ecliptic Latitude	0.449
Galactic Longitude (l^G)	0.182
Galactic Latitude (b^G)	0.540
Supergalactic Longitude (l^{SG})	0.654
Supergalactic Latitude (b^{SG})	0.167

4. Discussion

4.1. Correlation with Galactic Halo

Kuzmin and Rubakov (1997) [22] and Berezinsky et al. (1997) [23] have suggested a cosmic-ray source model associated with Dark Matter distribution in our galactic halo. In this model, most energetic cosmic rays are generated through decay of supermassive particles which are trapped in the galactic halo and thus distribute symmetrically around the galactic center. The arrival directions of most energetic cosmic rays, therefore, exhibit anisotropy at the Earth [39]. From recent studies by Berezinsky

and Mikhailov (1998) [35] and Medina Tanco and Watson (1998) [40], a significant anisotropy would be expected in the first harmonics of right ascension distribution, the amplitude of 40 % at phase about 250°, which is independent of the ISO and NFW models of dark matter distribution in the galactic halo. The ISO and NFW models are described in Kravtsov et al. (1997) [41] and Navarro, Frenk and White (1997) [42], respectively. This expected anisotropy is consistent with the results of the harmonic analysis above 4×10^{19}eV as shown in Figure 3. However, this amplitude is explained with statistical fluctuation of an isotropic distribution.

Table 6. Reduced-χ^2 values of the $\cos(\theta_{GC})$ distribution with three models.

	$\geq 1 \times 10^{19}$eV	$\geq 2 \times 10^{19}$eV	$\geq 4 \times 10^{19}$eV
isotropic distribution	2.0	1.7	1.8
ISO model	11.8	2.2	1.7
NFW model	10.0	1.9	1.6

As shown by the dashed and dotted curves in Figure 7, the ISO and NFW models of Dark Matter distribution in the galactic halo lead excess toward the galactic center. Table 6 shows the reduced-χ^2 values of the observed $\cos(\theta_{GC})$ distribution with the isotropic, ISO and NFW models. Although the distribution expected from the ISO and NFW models are quite different from the observed distribution in energies above 10^{19}eV, the reduced-χ^2 values are close to one another above 2×10^{19}eV and 4×10^{19}eV. Above 2×10^{19}eV, all three models are acceptable and it is hard to distinguish one from another.

4.2. Correlation with Nearby Galaxies

In Section 3.5, we calculated the chance probability of observing clusters under an isotropic distribution. If cosmic rays are astrophysical source origin, the non-uniform distribution of galaxies or luminous matters should be taken into account, as claimed by Medina Tanco (1998) [43]. He calculated trajectories of cosmic rays above 4×10^{19}eV in the intergalactic magnetic field under the assumption that flux of cosmic rays is proportional to the local density of galaxies. The expected distribution of cosmic-ray intensity is no more uniform and this may result in a strong anisotropy. This is different from the results in this paper so that our estimation of the chance probability of observing clusters under an isotropic distribution is experimentally reliable. However, his calculation shows important results: the C2 cluster is on top of a maximum of the arrival probability for sources located between 20 and 50 Mpc; and the C1 cluster locates on a high arrival probability region for sources at more than 50 Mpc. This suggests the possibility that the members of these clusters are generated at different sources. One need accumulate further statistics to make arrival direction, time and energy relation to be clear [43, 44] to distinguish whether the members of clusters come from a single source or unrelated sources.

4.3. Correlation with the Known Astrophysical Objects

As mentioned in Section 3.5, the BC1 cluster is in the direction of the Cygnus Loop (NGC6992/95). From the Hillas confinement condition of (magnetic field × size) for cosmic ray acceleration [45], the magnetic field in the shock of the Cygnus Loop is too small to accelerate cosmic rays up to 10^{19}eV. And the observed energy distribution and bunch of arrival time of the cluster members don't favor the diffusive shock acceleration. Another possible candidate is PSR 2053+36 with the period of 0.2215 sec and the magnetic field of about 3×10^{11} gauss [46]. It may be plausible that such highly magnetized pulsar has accelerated cosmic rays up to 10^{19}eV within a short time [47, 48]. It is highly desired to search for any signals from this direction in other energy range around MJD 50,000.

Table 7. Astrophysical objects near the AGASA events.

Event ID	Astrophysical object
C1	Mrk 359 (z = 0.017)
C2	NGC 3642 (z = 0.005), Mrk 40 (z = 0.02), Mrk 171 (z = 0.01)
970330 (1.5×10^{20}eV)	H 1934−063 (z = 0.011)

For the C1 – C5 clusters and 10^{20}eV cosmic rays, coincidence with known astrophysical objects are searched for from three catalogs which are the second EGRET catalog [49, 50], the CfA redshift catalog [51], and the eighth extragalactic redshift catalog [52]. The selection criteria are the following: (i) the separation angles within 4.0° from a member of each cluster, and 2.5° for the 10^{20}eV cosmic ray; (ii) the redshift within 0.02. In the CfA catalog, only QSOs/AGNs are selected. Candidate objects are listed in Table 7. Out of these objects, Mrk 40 (VV 141, Arp 151) is an interacting galaxy and may be most interesting. It should be noted that Al-Dargazelli et al. (1996) [53] claimed that nearby colliding galaxies are most favored as the sources of clusters (regions of excess events) defined by them using the world data available before 1996.

5. Summary

In conclusion, the cosmic-ray energy spectrum extends beyond 10^{20}eV. There is no statistically significant large-scale anisotropy related to the galactic nor supergalactic plane. The slight supergalactic plane enhancement is observed just above 10^{19}eV and arises mainly from the BC2 and C2 clusters. Above 4×10^{19}eV, one triplet and three doublets are found and the probability of observing these clusters by a chance coincidence is smaller than 1 %. Especially the triplet is observed against expected 0.05 events. Out of these clusters, the C2 (AGASA triplet) and C1 (doublet including the AGASA highest energy event or triplet together with the Haverah Park 10^{20}eV event) clusters are most interesting; they are triplets found in the world data sets and are located near the supergalactic plane. One should wait for the further high-rate observation to distinguish whether the members of clusters come from a single source or different sources. The $\cos(\theta_{GC})$ distribution expected from the Dark Matter

Halo model fits the data as well as an isotropic distribution above 2×10^{19}eV and 4×10^{19}eV, but is a poorer fit than isotropy above 10^{19}eV. The arrival direction distribution of the 10^{20}eV cosmic rays is consistent with that of lower energy cosmic rays and is uniform. It is noteworthy that three of seven 10^{20}eV cosmic rays are members of doublets. The BC1 cluster is in the direction of the Cygnus Loop or PSR 2053+36 region. It is desirable to examine any signals from this direction in other energy band around MJD 50,000.

Acknowledgments

We are grateful to Akeno-mura, Nirasaki-shi, Sudama-cho, Nagasaka-cho, Ohizumi-mura, Tokyo Electric Power Co. and Nihon Telegram and Telephone Co. for their kind cooperation. The authors are indebted to other members of the Akeno group in the maintenance of the AGASA array. M.Takeda acknowledges the receipt of JSPS Research Fellowships.

References

[1] M. A. Lawrence, R. J. O. Reid, and A. A. Watson, *J. Phys. G: Nucl. Phys.* **17**, 733 (1991).
[2] N. N. Efimov *et al.*, *Astrophysicsal Aspects of the Most Energetic Cosmic Rays*, eds. M. Nagano and F. Takahara (World Scientific, 1991) p.20.
[3] D. J. Bird *et al.*, *ApJ*, **424**, 491 (1994).
[4] S. Yoshida *et al.*, *Astropart. Phys.*, **3**, 105 (1995).
[5] M. Takeda *et al.*, *Phys. Rev. Lett.*, **81**, 1163 (1998).
[6] K. Greisen, *Phys. Rev. Lett.*, **16**, 748 (1966).
[7] G. T. Zatsepin, and V. A. Kuz'min, *Zh. Eksp. Teor. Fiz.*, **4**, 114 (1966) [JETP Letters, 4, 78].
[8] C. T. Hill and D. N. Schramm, *Phys. Rev.*, **D 31**, 564 (1985).
[9] V. Berezinsky and S. I. Grigor'eve, *A & A*, **199**, 1 (1988).
[10] S. Yoshida and M. Teshima, *Prog. Theor. Phys.*, **89**, 833 (1993).
[11] P. L. Biermann and P. A. Strittmatter, *ApJ*, **322**, 643 (1987).
[12] F. Takahara, *Prog. Theor. Phys.*, **83**, 1071L (1990).
[13] P. Rachen and P. L. Biermann, *A & A*, **272**, 161 (1993).
[14] M. Ostrowski, *A & A*, **335**, 134 (1998).
[15] R. D. Blanford, *MNRAS*, **176**, 465 (1976).
[16] R. V. E. Lovelace, *Nature*, **262**, 649 (1976).
[17] M. J. Rees *et al.*. *Nature*, **295**, 17 (1982).
[18] H. Kang, P. Rachen and P. L. Biermann, *MNRAS*, **286**, 257 (1997).
[19] M. Vietri, *ApJ*, **453**, 883 (1995).
[20] E. Waxman, *Phys. Rev. Lett.*, **75**, 386 (1995).
[21] P. Bhattacharjee and G. Sigl, *astro-ph/9811011* (1998).
[22] V. A. Kuzmin and V. A. Rubakov, *Phys. Atom. Nucl.*, **61**, 1028 (1998) [Yad. Fiz. 61, 1122].
[23] V. Berezinsky, M. Kachelriess and A. Vilenkin, *Phys. Rev. Lett.*, **79** 4302 (1997).
[24] N. Chiba *et al.*, *Nucl. Instr. and Meth.*, **A 311**, 338 (1992).
[25] H. Ohoka *et al.*, *Nucl. Instr. and Meth.*, **A 385**, 268 (1997).
[26] M. Teshima *et al.*, *Nucl. Instr. and Meth.*, **A 247**, 399 (1986).
[27] A. M. Hillas *et al.*, in *Proceedings of the 12th International Cosmic Ray Conference*, Hobart, **Vol. 3**, p. 1001 (1971).
[28] S. Yoshida *et al.*, *J. Phys. G:Nucl. Part. Phys.*, 20, 651 (1994).
[29] T. Doi *et al.*, in *Proceedings of the 24th International Cosmic Ray Conference*, Rome, **Vol. 2**, p. 764 (1995).
[30] N. Sakaki *et al.*, *in preparation.*
[31] H. Y. Dai *et al.*, *J. Phys. G: Nucl. Phys.*, **14**, 793 (1988).
[32] M. Nagano *et al.*, *J. Phys. G: Nucl. Phys.*, **18**, 423 (1992).
[33] N. Hayashida *et al.*, *Astropart. Phys.*, *to be published* (1999).
[34] J. Wdowczyk and A. W. Wolfendale, *J. Phys. G: Nucl. Phys.*, **10**, 1453 (1984).
[35] V. Berezinsky and A. Mikhailov, *astro-ph/9810277* (1998).
[36] N. Hayashida *et al.*, *Phys. Rev. Lett.*, **77**, 1000 (1996).

[37] W. H. Press *et al.*, in *NUMERICAL RECIPES in C*, (Cambridge University Press, 1988).
[38] T. Stanev and H. P. Vankov, *Phys. Rev.*, **D 55**, 1365 (1997).
[39] V. Berezinsky, *Nucl. Phys. Proc. Suppl.*, **70**, 419 (1998).
[40] G. A. Medina Tanco and A. A. Watson, *Astropart. Phys.*, *to be published* (1998).
[41] A. V. Kravtsov *et al.*, *ApJ*, **502**, 48 (1998).
[42] J. F. Navarro, C. S. Frenk and S. D. M. White, *ApJ*, **490**, 493 (1997).
[43] G. A. Medina Tanco, *astro-ph/9801060* (1998).
[44] G. Sigl and M. Lemoine, *Astropart. Phys.*, **9**, 65 (1998).
[45] A. M. Hillas, *Ann. Rev. Astr. Ap.*, **22**, 425 (1984).
[46] R. N. Manchester and J. H. Taylor, *ApJ*, **86**, 1953 (1981).
[47] J. E. Gunn and J. P. Ostriker, *Phys. Rev. Lett.*, **22**, 728 (1969).
[48] P. Goldreich and W. H. Julian, *ApJ*, **157**, 869 (1969).
[49] D. J. Thompson *et al.*, *ApJS*, **101**, 259 (1995).
[50] D. J. Thompson *et al.*, *ApJS*, **107**, 227 (1996).
[51] J. P. Huchra *et al.*, Harvard-Smithsonian Center for Astrophysics (1995).
[52] M. P. Veron-Cetty and P. Veron, ESO Scientific Report 18 (1998).
[53] S. S. Al-Dargazelli *et al.*, *J. Phys. G: Nucl. Phys.*, **22**, 1825 (1996).